NON-DESTRUCTIVE CHARACTERIZATION OF ADDITIVELY MANUFACTURED COMPONENTS USING X-RAY MICRO-COMPUTED TOMOGRAPHY

Stefan Dietrich*, Lukas Englert*, Pascal Pinter*
* Institute for Applied Materials (IAM-WK), Karlsruhe Institute of Technology (KIT), Karlsruhe, Germany

Abstract

Quality control and microstructure characterization are essential corner stones of the process optimization through the understanding of process-microstructure-relations in additive manufacturing. The scope of this work is to investigate the relationships between porosity and the process parameters as well as component geometry based on X-ray micro-computed tomography data and thus improving the ability for improved process control. Using test geometries manufactured via laser beam manufacturing and metal fused filament fabrication in combination with specialized image analysis and data fusion algorithms an extensive analysis of pore morphology, position and orientation with respect to the printing path could be carried out. The results show a clear connection between printing strategies as well as part geometry and allow for a direct connection to mechanical performance characteristics determined by the pore architecture like for example fatigue and failure behavior.

Keywords: Porosity Analysis, X-ray Computed Tomography, Laser Powder Bed Fusion, Metal FFF

Introduction

In order to achieve the transition of additive manufacturing (AM) processes from a pure development tool in prototype construction to production-ready solutions, the investigation of relations between process variables and the micro- and mesostructure of the manufactured components and materials are a decisive step. At the same time there is an increasing need for quality assurance and qualification measures of additively manufactured components to be able to use them in small series, especially in the aerospace industry [1, 2]. Nevertheless, new challenges have to be mastered when testing additively manufactured components via Non-destructive material testing and quantitative microstructure characterization (NDE). These include the intercorrelation of geometric features with the surface condition and respective tolerable defect sizes and types in the part. A comparative study by NASA [3] reveals the problems and deficiencies of some NDE methods, such as ultrasound methods, eddy current testing or color penetration methods, with the special state of an additively manufactured part in mind [4-5]. In this regard it is important to know the process-dependent critical defect sizes and to adequately evaluate the process variance and the component quality with sufficient measurement resolution and accessibility [3]. NDE therefore is often carried out by micro-computed tomography (μCT) in the scientific and industrial community. The specialties regarding the above mentioned necessities have not been systematically and quantitatively validated for additive materials [6]. As a quantitative and versatile NDE method, μCT has been used in some studies regarding additive manufacturing [3, 7, 8]. This is mostly due to both, the possibility of making internal structures of components accessible on a wide variety of scales from the cm to the μm range, as well as the various possibilities of automated 3D microstructure evaluation. Nonetheless the lack of adaption to additively manufactured microstructures delays the insight into process-structure-property relations with the aid of μCT in comparison to other complex materials like e. g. composites. Therefore, there is a need of further methodological development and implementation with further secondary information of the AM process.

Often computer tomography in the field of additive manufacturing has hitherto only been used to determine the porosity in an integral form or for the detection of pores in certain areas. Especially in the case of complex and safety-relevant components, the classification of defects and cracks with regard to their effects on the functional capability of the component is particularly crucial. Accordingly, the tolerances with respect to defect structures (critical initial flaw sizes - CIFS) are often narrowly defined (see, for example, [9]). Non-destructive testing and qualification for the detection of new defect types and damage mechanisms is a fundamental step in the further spread of additive manufacturing methods and components made from them.

A first process-dependent description of the global pore architecture has already been successfully performed by μCT investigations on samples prepared via electron beam melting, but without reference to the resulting

mechanical properties [10]. Here, a direct correlation between pore shape, pore position and the derivable history of gas bubble inclusions during the different contour or hatch steps could be found. The influence of certain orientation distributions, positions, and pore sizes on the mechanical properties has already been explored in several papers [11-13] by examining individual aspects. In this case, however, the correlation of various characteristics of the pore architecture as well as the link with the process control and the local component geometry has not been carried out comprehensively. Therefore, no link could yet be established between the variables describing the pore architecture and the deformation and failure-relevant component properties.

Compared to the possibilities that have been developed, for example, in the area of fiber-reinforced composite materials, these number of investigations is significantly less in the case of additive-produced metallic materials (see for example [14,15]). The methods developed for process-dependent fiber orientation analysis, component geometry-dependent pore analysis and crack detection allow significantly more extensive process control and quality assurance in production. The transferability of such methods to the detection of microstructural features on metallic materials as process-dependent variables in additively manufactured components therefore constitutes a field of research largely untapped.

Experimental Methodology

Additive Manufacturing

Within this work two different additive manufacturing methods have been used to investigate process symptomatic porosity. On the one hand side parts were printed out of AlSi10Mg on an SLM Solutions 280-HL machine using the standard parameters provided by the SLM build processor to the Materialize interface (see Figure 1 left, middle). Therein a hatch spacing of 170 µm has been used for the border contour, the fill contour as well as the hatching. The laser power was 300, 250 and 350 W and the laser speed 600, 555, 1150 mm/s respectively. Hatching in each layer was rotated by 67 ° with a layer height of 50 µm. The CuCr1Zr coil for the local thickness evaluation was manufactured according to the optimal parameters for the material published by [16] at ILT Aachen, Germany.

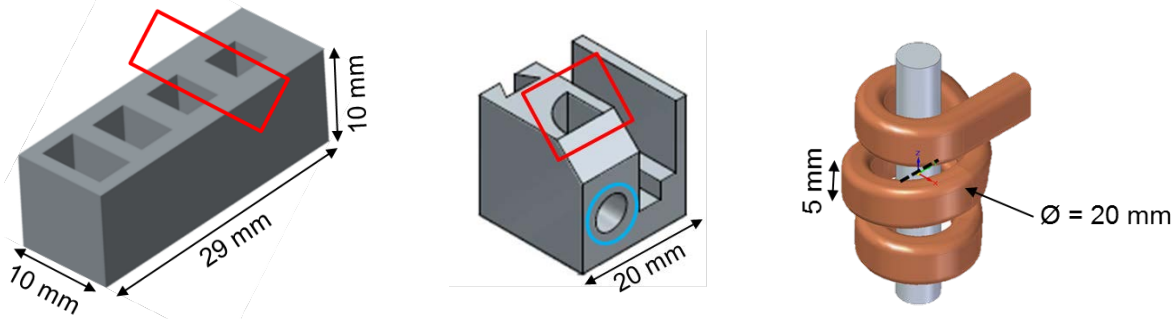

Figure 1: Sample geometries investigated from the laser beam melting process (LBM) out of AlSi10Mg (left, middle) for porosity (red detail) and surface roughness (blue circle) analysis and CuCr1Zr (right) for local thickness analysis.

Additionally, metal fused filament fabrication (FFF) was carried out using the Ultrafuse 316L filament with a diameter of 1.75 mm and an 80 % metal filling on a P220 FFF printer (Apium Additive Technologies GmbH) with a heated base plate at 120 °C and a nozzle (Ø 0.4 mm) at 210 °C. The hatch distance was 480 µm, the layer height 100 µm and the printing speed was set to 2000 mm/min. The so produced green part is then subjected to BASFs catalytic debinding process creating the brown part and the final vacuum sintering step at 1360 °C creating the finished metal part.

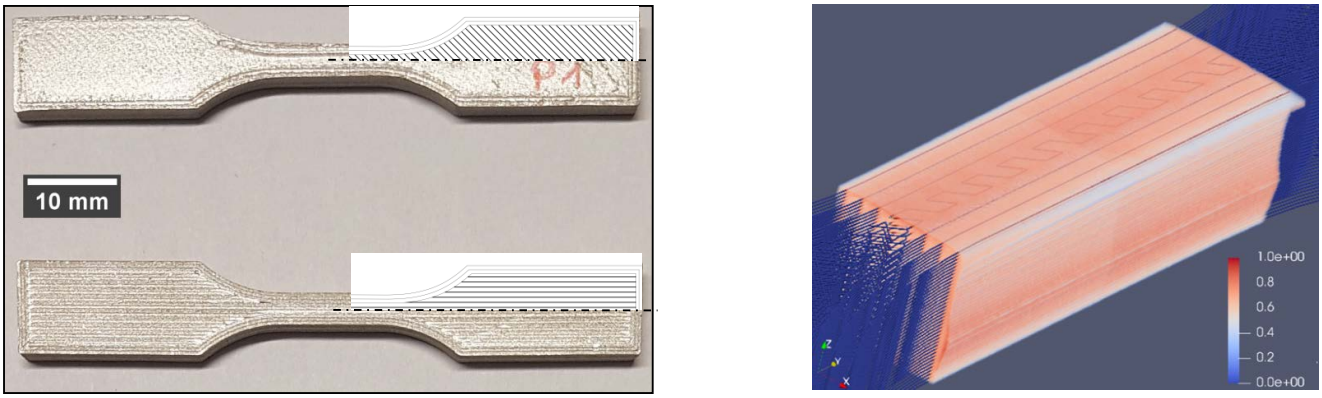

Figure 2: Differently hatched 316L FFF samples with three contours and 45° as well as 0° hatching orientation (left) and composite image visualizing the G-code for the print head movement registered and overlaid with the µCT image.

Micro-Computed Tomography (µCT)

The µCT images have been acquired on a YXLON Y.CT-Precision µCT system with a micro-focus X-ray tube in reflection mode. The scanning parameters of the system have been adjusted for each material and sample size in order to increase resolution while still retaining a representative sample volume. According parameters for each material are presented in Table 1.

Table 1: Scanning parameters for the different geometries and materials of the samples investigated.

Material	Source Voltage	Target Current	Equiv. Diameter	Scan Speed	Resolution
AlSi10Mg	160 kV	0.06 mA	14 mm	0.4 h/cm	10 µm
316L	160 kV	0.15 mA	7 mm	0.6 h/cm	4 µm
CuCr1Zr	150 kV	0.15 mA	16 mm	0.7 h/cm	6 µm

The projection data was reconstructed using the standard Feldkamp-Davis-Kress (FDK) algorithm. The resulting 16-bit gray value images are then binarized for the image analysis using a local thresholding algorithm after Phansalkar [17]. The gray value or binarized images are the input data for each of the algorithms described in the following section.

3D Microstructure Analysis

Data Fusion in 3D Printing

In order to connect the information about the additive manufacturing process like laser path or print head path with the microstructural information of the so created part, it is necessary to overlay the image data from computed tomography with the data of the slicing process which creates the layer-wise structure of the AM part. To this end the slice data in form of slice views in closed systems or the G-code from open systems is stacked to create 3-dimensional data similar to the data reconstructed from the µCT. The paths of the laser or the print head can then be visualized as lines or vectors indicating directional features and correlations of the process in the entire part discriminating equally different printing strategies for different regions. Furthermore, it is possible to resliced the 3D data along the path and measure e.g. local density on zones along the path. In order to co-analyze the µCT image with the stacked layer from slicing an alignment of the CAD part with the µCT image is achieved via standard 3D image registration, which can be found in most imaging libraries (e.g. ITK) or commercial software suites like Avizo or VGStudioMAX.

Local Curvature

The local curvature of a three-dimensional object is characterized by the two principal curvatures κ_1 and κ_2 as the maximum and minimum normal curvature which represent the reciprocal of the local radius at a point $\vec{p}$(x,y,z) of the surface. Since the curvature is often used to give a direct surface description independent of the coordinate system the mean curvature as the arithmetic mean of the principal curvatures is calculated by $H=0.5(\kappa_1 + \kappa_2)$. Another common description is the Gaussian curvature as the product of the two principal curvatures with $K= \kappa_1 \bullet \kappa_2$.
In this work, the maximum curvature $\max(\kappa_1, \kappa_2)$ is considered, because it can be unambiguously visualized and connected to a notch effect around the pore metal interface in contrast to the Gaussian or mean curvature which can cancel out at saddle points or cylindrical surfaces. The method used to calculate the local curvature on the binarized image is based on the local Hessian matrix that can be calculated directly from the voxel data

$$HG(x,y,z) = \begin{bmatrix} \frac{\partial^2 G}{\partial x \partial x} & \frac{\partial^2 G}{\partial x \partial y} & \frac{\partial^2 G}{\partial x \partial z} \\ \frac{\partial^2 G}{\partial y \partial x} & \frac{\partial^2 G}{\partial y \partial y} & \frac{\partial^2 G}{\partial y \partial z} \\ \frac{\partial^2 G}{\partial z \partial x} & \frac{\partial^2 G}{\partial z \partial y} & \frac{\partial^2 G}{\partial z \partial z} \end{bmatrix}$$

$G(x,y,z)$
Several researchers showed that the local principal curvatures can be calculated by solving the eigenvalues of the Weingarten map in matrix form (see e.g. [18])

$$l = \frac{1}{\|\Delta G(p)\|} \begin{bmatrix} \boldsymbol{b_1^t} HG(p) \boldsymbol{b_1} & \boldsymbol{b_1^t} HG(p) \boldsymbol{b_2} \\ \boldsymbol{b_2^t} HG(p) \boldsymbol{b_1} & \boldsymbol{b_2^t} HG(p) \boldsymbol{b_2} \end{bmatrix}$$

Where **b1** and **b2** are arbitrary orthonormal basis vectors for the tangent plane on the surface at the point $\vec{p}$(x,y,z) where the surface of the pore can be found after an edge detection based on the spatial derivatives of the object.

Local Thickness

The local thickness of an object can be plainly described as the maximum radius of a sphere that can be moved through a structure in any direction [19]. The mathematical equation describing this property of a 3D object is then given by

$$\tau(\vec{p}) = 2\max(\{r | \vec{p} \in \mathrm{sph}(\vec{x}, r) \subseteq \Omega, \vec{x} \in \Omega\})$$

Numerically this property is derived using several algorithms commonly known in image analysis and available in most softwares.These are a distance transformation to produce the distance map D, skeletonization of the distance map to produce the distance ridge q by removing redundant points of the distance map and computation of the local thickness by scanning the distance ridge at each point $\vec{p}$ for the largest value q containing $\vec{p}$ in its sphere with radius r equal to q.

Roughness/Waviness on Complex Surfaces

The surface quality including waviness and roughness in additively manufactured parts is a geometry and process parameter dependent property of each part and is difficult to access for in most cases complex geometries realized in AM. Therefore, in this work algorithms using the surface points after an edge detection step for a 3D surface fitting with polynomials of order four or, if the target shape can be easily described, geometric primites (e.g. cylinders, spheres) are used to calculate the distance of these points from the “mean surface” characterized by the fit. The evaluation of roughness and waviness then follows DIN 4287 producing comparable Ra and Rz values from the roughness peak and valley distances in the local neighborhood of the fitted surface.

Results

The results for the different image analysis algorithms will be given on exemplary sections of the manufactured specimen in order to simplify the finding of structure-property relations. The results for different image analysis methods will be given according to the methodological section explaining the mathematical approaches behind each algorithm. This is not intended to be a comprehensive investigation of fundamental AM properties but rather exemplary applications where the algorithms provide improved insight into AM process-structure-property relations.

Data Fusion in 3D Printing

After data fusion of the µCT image with the hatching and perimeter path according to the method described in the last section, a global analysis of the porosity distribution and orientation has been conducted. For that purpose, a projection of the porosity along the build direction (see Figure 3 left) shows zones of high and low porosity clearly reflecting the outer shape of the manufactured part. By comparing the porosity concentrations with the laser path there is no indication of porosity creation at the interface between hatching and perimeter since the highest concentration of pores is about 0.3 mm within the hatching zone. Furthermore, a calculation of global main orientations of the single pores using a principal component analysis (PCA) clearly shows the orientation of the majority of pores along the horizontal surface (azimuthal angle 0°) coinciding with the porosity seam visible in the projection image. The frequency of out of the build plane orientations (elevation angle) is rather evenly distributed between ± 60° and sharply drops to zero approaching the 90° angle representing an orientation along the build direction (see Figure 3 right).

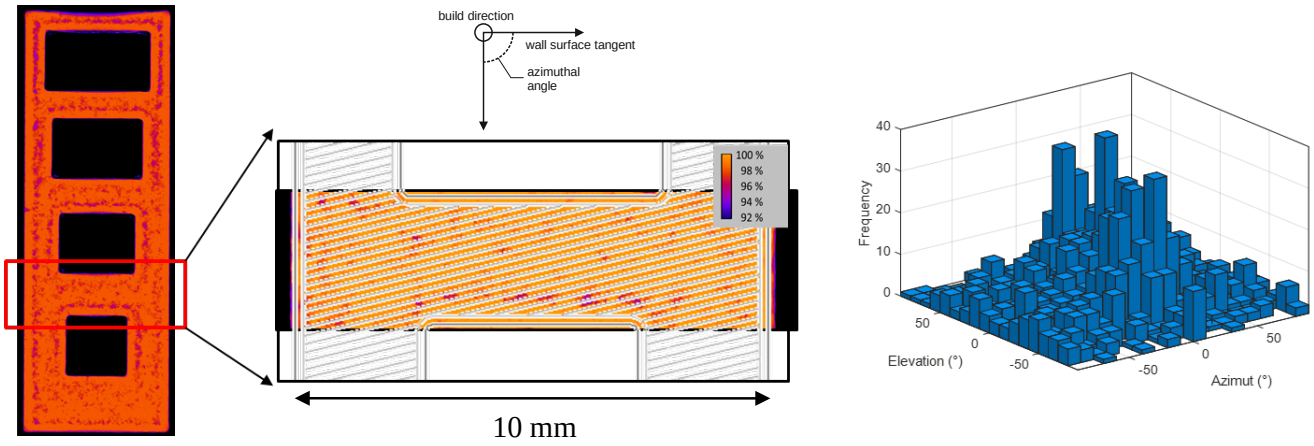

Figure 3: Global porosity distribution in the test geometry in relation to the surface and hatching zones of the part (left) and angular distribution of azimuthal (in layer) angle and elevation (out-of-layer) angle in the highlighted wall (right).

This drop in frequency with a main orientation along the build direction is reduced if the pores are aligned with the walls horizontal surface tangent direction and are tilted around the normal direction standing on the build orientation and the wall surface tangent (see also Figure 4 left).

In order to further investigate the correlation not only with the perimeter and hatching zones but also the layer wise change in hatching orientation, the mean orientation of the pores in each layer was evaluated and directly compared to the hatching orientation of the associated built layer in Figure 4 (right). Overlapping points represent layers with coinciding orientations mostly governed by a few aligned pores in these layers. This data does not necessarily imply that the porosity alignes with the hatching path orientation everywhere inside the part but the reverse conclusion turns out to be true. If in a layer the main orientations between porosity and hatching direction coincide this is mainly due to a few large aligned pores in this direction.

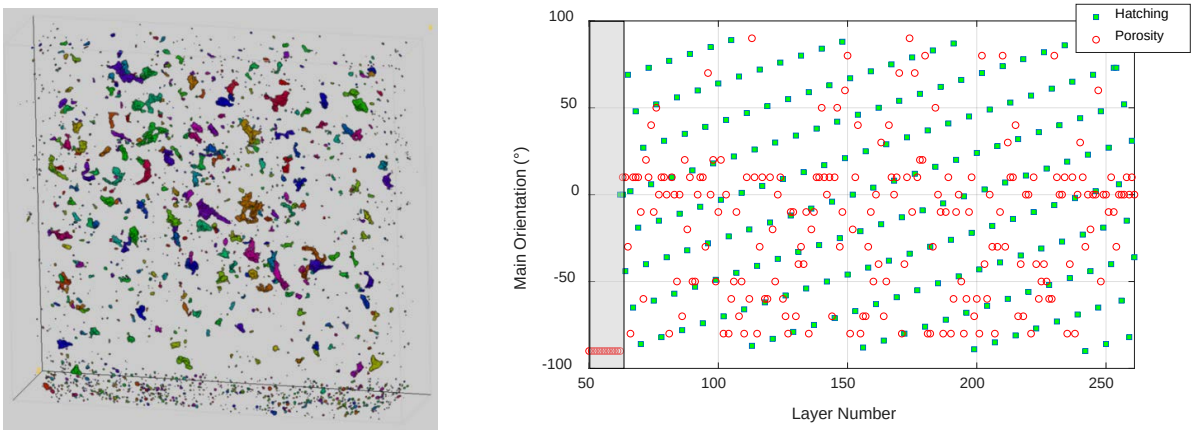

Figure 4: Porosity in the highlighted wall of first test body (left) and correlation between pore main orientation and hatching orientation for each layer (right).

In contrast to the LBM process the porosity in the metal FFF process shows a distinctive orientation correlation to the path of the print head and the printing strategy. The orientation of pores in the two representative printing strategies investigated herein clearly reproduces the track offset even after sintering of the final sample. This is for both the 0° and 45° samples visible in the equidistant position of most of the porosity in pore channels along the 0° hatching direction (see Figure 5 left) and in the wedge like porosity at the interface of perimeter and 45° hatching (see Figure 5 right).

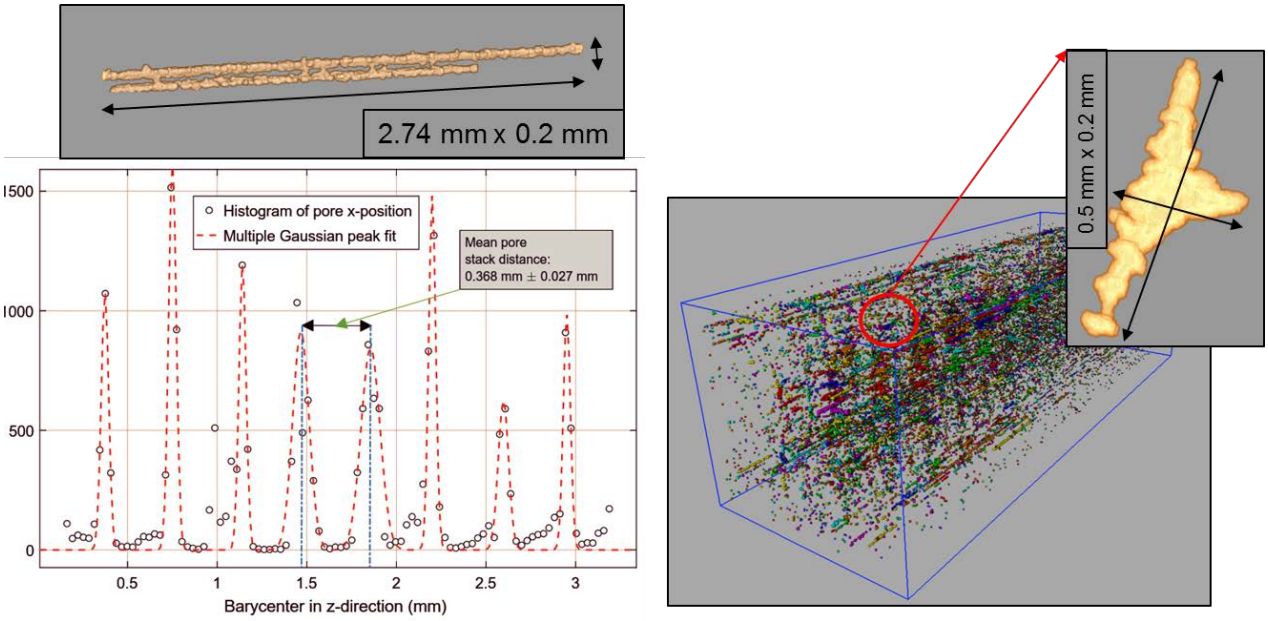

Figure 5: Distribution of pores in the metal FFF tensile test samples with a 0° hatch orientation (left) showing long pore channels at nearly the distance between subsequent tracks. For a 45° hatch orientation the typical pore shape at the intersection of the hatch and the contour lines (right) exhibits a wedge like shape and similar pore channels like in the 0° orientation between the three contour lines.

Local Curvature

The local curvature calculated using the Hessian based method outlined before can give further insight into the shape of the pores and their effect on mechanical properties. For this purpose the maximum curvature is color coded in comparison to an isosurface visualization (Figure 6 left) with regions of positive curvature in red and regions of negative curvature in green. Applying the algorithm to the entire wall it is possible to classify the

porosity according to their amount of positive curvature resulting in a notch effect in the surrounding material (see Figure 6). Using these curvature histograms available now for each pore surface also a geometrical classification is possible. This classification with the fraction of high curvature in relation to for example the volume of the pore or the closest position to the part surface allows for the detection of hot spots regarding failure probability. In Figure 6 (right) for the wall considered from the AlSi10Mg test geometry, the pore indicated by the black rectangle has the highest positive mean curvature per volume and the lowest distance from the part surface. Depending on the load case, this pore would be the initiation point of failure with a high certainty. Similar shape classifications are then especially important for the fatigue behavior as e. g. indicated in [21].

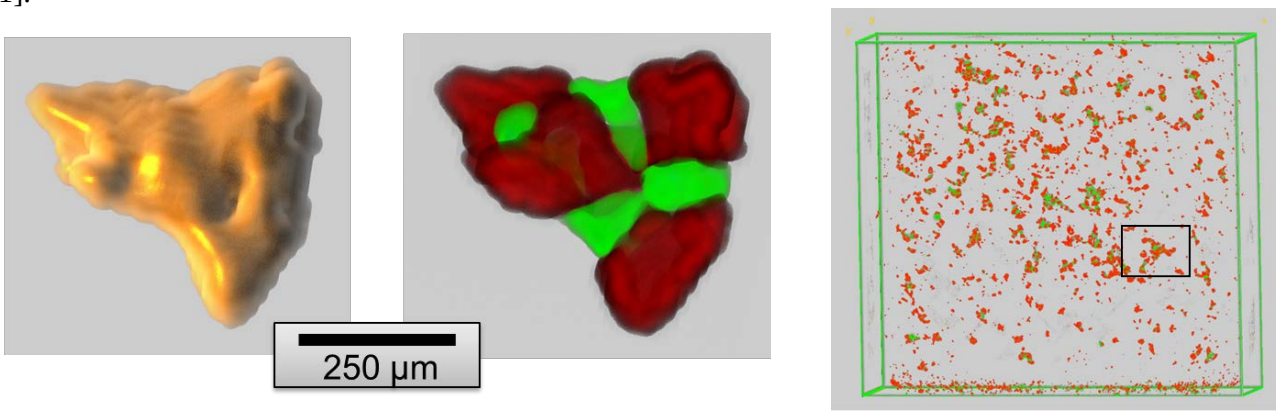

Figure 6: Curvature visualization discriminating between positive (red) and negative (green) curvature on the surface area of a pore.

Local Thickness

The calculation of the local thickness distribution is best shown on a part where the residual wall thickness plays an important role for the functioning of the part. The copper coil with a cooling channel circulated by pressurized water has to be impermeable in order to guarantee the function of the heating coil. It is obvious that also in the LBM process for the copper alloy a seam of porosity with dependence to the geometry is created weakening the wall material of the cooling channel and, as a secondary effect, reducing the conductibility of the copper material lowering the electro-magnetic performance of the heating system (see Figure 7).

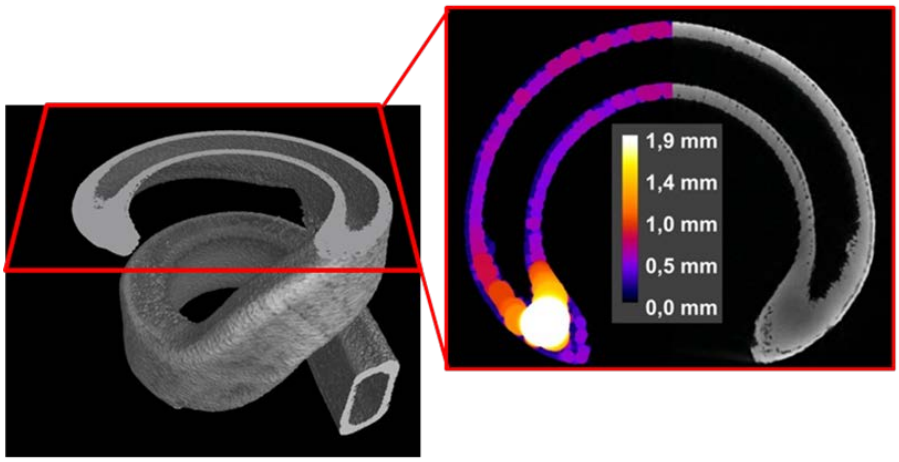

Figure 7: Visualization of the LBM copper coil cooling channel within the µCT scan including a cut through the part and the two-dimensional local thickness analysis indicating the residual wall thickness.

Evaluating the local thickness across the part a large range of local thickness values can be found indicating zones of low porosity as well as thin walls between the porosity seam and the part surface with a minimal thickness of only 0.25 mm.

Roughness/Waviness on Complex Surfaces

The application of the roughness measurements from µCT image data on the test geometry with a cylindrical cavity is outlined in Figure 8. It is obvious that the overhanging part of the cavity exhibits peak maxima with Rt of nearly 600 µm after DIN ISO 4287 (see e.g. Figure 8 right). The correction of the cylindrical geometry through the fitting of a cylindrical surface to the image data was described in the section before and allows for a planar visualization of the unrolled part surface in the cavity (see e. g. Figure 8 right).

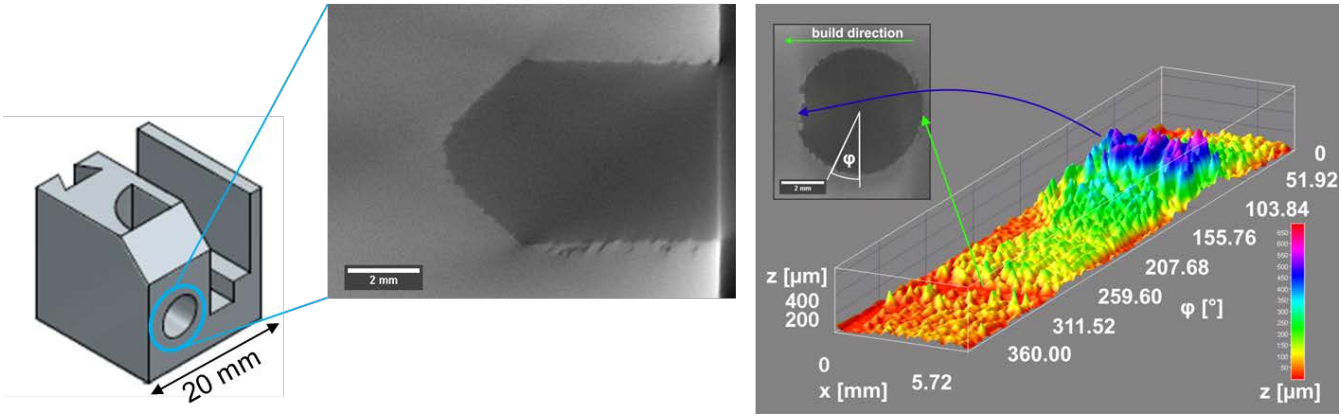

Figure 8: Roughness on the mantle surface of a printed cylindrical hole in a geometric test specimen

Discussion

The techniques described in this work show the advantage of a data fusion based approach to investigate process-microstructure–property relations in additively manufactured materials. For such a data fusion procedure to work it is at first necessary to be able to access the machine data in an automatic data analysis format such as 3D image data or vectorized G-code, as indicated above. The herein used machine data for open and closed systems was translated into 3D path data in order to analyze the microstructural data along these paths and enables the correlation of porosity characteristics to the machine path. For the LBM samples certain directions of the hatching relative to the perimeter show strong orientation connections although only the largest pores are clearly aligned in a layer and are also accompanied by randomly oriented smaller porosity. For the metal FFF samples the connection is more distinctive and shows large pore channels along the print head path. The typical shape of the porosity in metal FFF can then be directly explained by the stacking of the filament paths since crossing paths create significantly smaller porosity and turning points in the path create wedge like pores following the path angles with their outer surface.
The curvature evaluation on the surface of single pores allows for a classification using the overall and spatial distribution of high curvature regions. Using this method on the geometry dependent large pores in additively manufactured parts producers can use the data in a process optimization as well as a 100 % quality control.
The local thickness evaluation for the detection of minimum residual wall thickness described in this work is especially valuable to describe the effects of close surface porosity, e.g. for LBM processes without skywriting strategies. As a method to detect weak spots in thin walled structures this method promises to increase the prediction ability of critical flaws in combination with the surface curvature classification and the relation to process parameters influenced by the laser or print head path.
For complex 3D parts roughness measurements using NDE methods are often prohibited due to restrictions in access to the surface. In this regard µCT measurements can help to measure the surface structure of e.g. cavities and inner surfaces using the surface point distances normal to the fitted surface representing the local geometry of the part. Nonetheless care must be taken of the resolution limit posed by the voxel size of the µCT image volume as discussed for example in [22]. Therefore, the method is only applicable for roughness values in the range of several µm.

Conclusions

The use of µCT measurements in the microstructure characterization and quality control of the process and final part poses a very versatile tool with the ability to detect local defects and classify or correlate those defects according to their criticality and evolution from the process. A key tool for this is the data fusion of µCT and process data which can be achieved e.g. by extraction of the laser path and registration of the spatial data sets on the 3D images. Furthermore, we could show three different image analysis algorithms especially useful for porous LBM materials or parts. Using the local curvature calculation on the surface of each pore allows to detect zones of high curvature and therefore increased danger of stress concentrations around these zones. This can be used to evaluate if process dependent porosity is still bearable or the part should be printed again. In the case of metal FFF materials a clear classification of the pore shape with curvature data is possible and is directly correlated to the extruder and print head path of the machine.

Acknowledgements

The authors would like to thank James Damon for his support in the evaluation of µCT images and the Rosswag GmbH, process engineering team for providing some of the LBM AlSi10Mg samples. Additionally, we like to thank Daniel Heußen for manufacturing the Cu inductor according to our designs at Fraunhofer ILT in Aachen.

References

[1] Airbus Defence and Space optimising components using 3D printing for new Eurostar E3000 satellite platforms. http://airbusdefenceandspace.com/newsroom/news-and-features/airbus-defence-and-space-optimising-components-using-3d-printing-for-new-eurostar-e3000-satellite-platforms/. Accessed 10 June 2015.

[2] GE Reports staff. 2015 The FAA Cleared the First 3D Printed Part to Fly in a Commercial Jet Engine from GE. http://www.gereports.com/post/116402870270/the-faa-cleared-the-first-3d-printed-part-to-fly.

[3] Jess M. Waller, Bradford H. Parker,Kenneth L. Hodges, Eric R. Burke, James L. Walker. 2014 Nondestructive Evaluation of Additive Manufacturing. State-of-the-Discipline Report. NASA/TM—2014–218560.

[4] Slotwinski, J. A., Garboczi, E. J. & Hebenstreit, K. M. 2014 Porosity Measurements and Analysis for Metal Additive Manufacturing Process Control. Journal of research of the National Institute of Standards and Technology 119, 494–528.

[5] Caiazzo, F., Cardaropoli, F., Alfieri, V., Sergi, V. & Cuccaro, L. 2013 Experimental analysis of selective laser melting process for Ti-6Al-4V turbine blade manufacturing. In XIX International Symposium on High-Power Laser Systems and Applications (ed. K. R. Allakhverdiev), p. 86771: SPIE.

[6] U.S. Department of Commerce. 2013 Measurement Science Roadmap for Metal-Based Additive Manufacturing.

[7] Ziółkowski, G., Chlebus, E., Szymczyk, P. & Kurzac, J. 2014 Application of X-ray CT method for discontinuity and porosity detection in 316L stainless steel parts produced with SLM technology. Archives of Civil and Mechanical Engineering 14, 608–614.

[8] Vasić, S., Grobéty, B., Kuebler, J., Graule, T. & Baumgartner, L. 2010 XRCT characterisation of Ti particles inside porous Al2O3. Materials Characterization 61, 653–660.

[9] NASA. 2008 Nondestructive Evaluation Requirements for Fracture-Critical Metallic Components. https://standards.nasa.gov/documents/detail/3315641. Accessed 11 June 2015.

[10] Tammas-Williams, S. 2015 XCT analysis of the influence of melt strategies on defect population in Ti–6Al–4V components manufactured by Selective Electron Beam Melting. Materials Characterization 102, 47–61.

[11] Aboulkhair, N. T., Everitt, N. M., Ashcroft, I. & Tuck, C. 2014 Reducing porosity in AlSi10Mg parts processed by selective laser melting. Additive Manufacturing 1-4, 77–86.

[12] Chin Ang, K., Fai Leong, K., Kai Chua, C. & Chandrasekaran, M. 2006 Investigation of the mechanical properties and porosity relationships in fused deposition modelling fabricated porous structures. Rapid Prototyping Journal 12, 100–105.

[13] Sudarmadji, N., Tan, J. Y., Leong, K. F., Chua, C. K. & Loh, Y. T. 2011 Investigation of the mechanical properties and porosity relationships in selective laser-sintered polyhedral for functionally graded scaffolds. Acta biomaterialia 7, 530–537.
[14] Robb, K., Wirjadi, O., & Schladitz, K. 2007. Fiber orientation estimation from 3D image data: Practical algorithms, visualization, and interpretation. In Hybrid Intelligent Systems, 2007. 7th International Conference on Hybrid Intelligent Systems (pp. 320-325). IEEE.
[15] Shen, H., Nutt, S. & Hull, D. 2004 Direct observation and measurement of fiber architecture in short fiber-polymer composite foam through micro-CT imaging. Composites Science and Technology 64, 2113–2120.
[16] Becker, D., Selektives Laserschmelzen von Kupfer und Kupferlegierungen; Dissertation, 2014, TH Aachen
[17] Phansalkar, N., More, S., Sabale, A. & Joshi, M. "Adaptive local thresholding for detection of nuclei in diversity stained cytology images," 2011 International Conference on Communications and Signal Processing, Calicut, 2011, 218-220.
[18] Hughes, J.F. 2003. Differential geometry of implicit surfaces in 3-space-a primer, Report, Department of Computer Science Brown University Providence, Rhode Island.
[19] Hildebrand, T., Rüesegger,P. 1996. A new method for the model-independent assessment of thickness in three-dimensional images. Journal of Microscopy, 185, 67-75.
[20] Dougherty, R., Kunzelmann, K. 2007. Computing local thickness of 3D structures with ImageJ. Microsc. Microanal., 13, 1678-1679.
[21] Damon, J., Dietrich, S., Schulze,V. 2018. Process dependent porosity and the influence of shot peening on porosity morphology regarding selective laser melted AlSi10Mg parts. Additive Manufacturing, Volume 20, 77-89.
[22] Kerckhofs, G., Pyka, G., Moesen, M., Schrooten, J. and Wevers, M., 2012, September. High-resolution micro-CT as a tool for 3D surface roughness measurement of 3D additive manufactured porous structures. In *iCT Conf* , 77-83.